Available online at www.sciencedirect.com
SCIENCE DIRECT®
Journal of Solid State Chemistry 179 (2006) 41–48
JOURNAL OF SOLID STATE CHEMISTRY
www.elsevier.com/locate/jssc

Effect of ultraviolet irradiation on crystallization behavior and surface microstructure of titania in the sol–gel process

Bifen Gao[a,c], Ying Ma[a], Yaan Cao[b], Jincai Zhao[a], Jiannian Yao[a,*]

[a]*Key Laboratory of Photochemistry, Institute of Chemistry, Chinese Academy of Sciences, Beijing 100080, PR China*
[b]*College of Physics, Nankai University, Tianjin 300071, PR China*
[c]*Graduated School of Chinese Academy of Science, PR China*

Received 15 July 2005; received in revised form 23 September 2005; accepted 24 September 2005
Available online 26 October 2005

Abstract

Nanosized titania was prepared at various hydrolysis ratios ($r = H_2O/Ti$) by photo-assisted and conventional sol–gel methods. It was found that hydrolysis ratio and ultraviolet irradiation greatly affect the titania crystallization behavior. The introduction of photo-irradiation benefits anatase formation throughout a wide range of hydrolysis ratio. XPS results show that hydrolysis reaction was promoted by ultraviolet irradiation. In addition, photo-irradiation was also verified to be in favor of the generation of large specific surface area and high crystallinity, which resulted in relative high photocatalytic activity of TiO_2 prepared by a photo-assisted sol–gel method.

Keywords: Titanium dioxide; Sol–gel process; Photo-irradiation; Crystallization; Photocatalysis; Surface microstructure; Anatase; Rutile; Hydrolysis; Condensation

1. Introduction

Titanium dioxide is a material of great importance due to useful electrochemical, dielectric, electroconductive, and optical properties. It is widely used as cosmetics, pigments, photocatalysts, adsorbents, catalytic supports, and sensors [1–3]. For these applications, the morphology, average particle size and particle size distribution, porosity, phase composition, and crystallinity of titania are important factors to be controlled. Among the various methods developed to prepare TiO_2 [4–10], sol–gel method is the most used since the sol–gel processing has a prominent advantage of the facile control of structures and properties of the product through simple alteration of processing parameters. Recently, many modified sol–gel processes have been applied in the preparation of nanosized TiO_2. Hydrothermal treatment has been demonstrated favorable for preparing ultrafine nanocrystalline TiO_2 without particle agglomeration [11] and anatase with a high thermal stability [12]. Yu et al. [13] synthesized highly photocatalytic active nanosized TiO_2 particles by hydrolysis of titanium tetraisopropoxide via ultrasonic irradiation.

Extensively applied in the photoreduced preparation of noble metal nanocrystals [14,15] and narrowing the size distribution of semiconductor nanoparticles [16,17], ultraviolet irradiation has also been used to densify and crystallize the sol–gel derived precursor films such as SiO_2, TiO_2, ZrO_2 and ZnO films [18–21] as an alternative method to calcination. In addition to thermal effect, ultraviolet laser has also been believed to induce electronic excitations during such post-treatment [19,21]. More recently, we developed a photo-assisted sol–gel method [22–24] in which titanium alkoxide was hydrolyzed in acidic medium under ultraviolet irradiation to prepare nanosized TiO_2 with high crystallinity and small crystallite size at relatively low calcination temperature. We found that the phase transitions from amorphous to anatase and anatase to rutile were promoted by ultraviolet light irradiation, and the photocatalytic activity of titania film prepared with photo-irradiation was much higher than that of the sample prepared without irradiation. However, the

*Corresponding author. Fax: +86 10 82616517.
E-mail address: jnyao@iccas.ac.cn (J. Yao).

0022-4596/$ - see front matter © 2005 Elsevier Inc. All rights reserved.
doi:10.1016/j.jssc.2005.09.039

general effects and mechanism of ultraviolet irradiation in the hydrolysis and condensation reactions are still not very clear. It is well known that the hydrolysis ratio ($r = H_2O$/metal), catalyst and complexing ligands are the main factors controlling the growth of transition metal oxides in the sol–gel process. So as to better understand the general effect of ultraviolet irradiation, we prepared nanosized TiO_2 at various hydrolysis ratios by photo-assisted and conventional sol–gel methods in this work. We found that ultraviolet irradiation has great effect on crystallization behavior and surface microstructure of TiO_2 in a wide range of hydrolysis ratio.

2. Experimental section

2.1. Materials preparation

All chemicals used in this study were of analytical grade and used without further purification. Titanium (IV) isopropoxide was supplied from Aldrich. The others were from Beijing Chemical Company. Millipore water (18.2 MΩ) was used in all experiments.

In a typical preparation of titania colloid, anhydrous 2-propanol solution (29 mL) containing 9 mL titanium (IV) isopropoxide was slowly added into 46.8 mL alcohol solution containing 3 mL hydrochloric acid and different amount of deionized water under vigorous stirring at room temperature. The hydrolysis ratio ($r = H_2O/Ti$) varied from 4 to 20. After mixing, the sol was stirred and illuminated for 15 h by a 375 W high-pressure mercury lamp. A Pyrex reactor was used to cut off light of wavelength shorter than 290 nm and a circulating water cuvette was used to avoid the heating effect of the lamp. The distance between the lamp and reactor was 15 cm and the intensity of the UV radiation reaching the reactor was about 4 mW cm^{-2}. Under the otherwise identical conditions, TiO_2 colloid was also prepared by a sol–gel method in the dark for comparison. Titania powders were prepared by evaporating solvent from the colloid at room temperature and then annealing the gel at different temperatures for 4 h. The samples prepared by a photo-assisted sol–gel method were denoted as R4-P, R7-P, R10-P and R20-P (the number labels the hydrolysis ratio and P represents photo-irradiation). The samples prepared in the dark were marked as R4-N, R7-N, R10-N and R20-N (the number labels the hydrolysis ratio and N represents non-irradiation).

2.2. Photocatalytic experiments

Rhodamine B (RB) was from Tokyo Kasei Kogyo Co. Ltd. and used as received. An aqueous suspension of RB (1.0×10^{-5} mol L^{-1}, 50 mL) and TiO_2 (2.5 mg) contained in a 80 mL Pyrex vessel was stirred for about 30 min in the dark to reach the adsorption/desorption equilibrium. Subsequently the dispersion was irradiated with ultraviolet light provided by a 375 W high-pressure mercury lamp. A 1.0 cm thick circulating water cuvette was used to remove the heat of the lamp. Variations in the concentration of the dye in the degraded solution were monitored by UV-Vis spectroscopy (Shimadzu UV-1601 PC).

2.3. Samples characterization

The XRD patterns were acquired on a Rigaku D/max 2500 X-ray diffraction spectrometer (Cu$K\alpha$, $\lambda = 1.54056$ Å) at a scan rate of 0.02° 2θ S^{-1}. The average crystallite size was calculated according to the Scherrer formula ($D = k\lambda/B\cos\theta$). The BET surface areas of the samples were determined by nitrogen adsorption–desorption isotherm measurement at 77 K. The samples annealed at 373 K were degassed at 100 °C prior to actual measurements. However, for the samples calcined at higher temperature, the degassing temperature was 180 °C. The average pore size was calculated from the desorption branch of the nitrogen isotherm by the BJH method. TEM samples were prepared by dispersing the powders in ethanol and then depositing onto carbon-coated copper grids. These samples were then observed with a JEOL-2010 electron microscope at an accelerating voltage of 200 KV. XPS measurements were carried out with an SECA Lab 220i-XL spectrometer by using an unmonochromated Al $K\alpha$ (1486.6 eV) X-ray source. All the spectra were calibrated to the binding energy of the adventitious C1 s peak at 284.6 eV. Thermogravimetric analyses (TGA) were carried out in a Perkin-Elmer thermoanalyze under dry air, using platinum crucibles and a constant heating rate of 10 °C min^{-1} up to 700 °C.

3. Results and discussion

Fig. 1 shows XRD patterns of TiO_2 powders prepared with and without UV irradiation followed by drying at 373 K. It can be seen that the crystallization behavior greatly depends on the hydrolysis ratios and photo-irradiation. Anatase is the main phase in most of the samples except for R7-N and R20-P. A small shoulder frequently occurring on the higher angle side of the anatase (1 0 1) peak indicates the presence of small amounts of brookite [25]. In the conventional sol–gel process, at low hydrolysis ratio ($r = 4$), only a trace amount of rutile is observed, while a large amount of rutile (about 87% of weight fraction according to the calculation method reported in Ref. [26]) is detected at $r = 7$. When the content of H_2O is increased further, anatase becomes the dominant crystalline phase again although amorphous phase is evidently present in the sample prepared at $r = 10$. In contrast, nearly pure anatase is acquired when the sols were irradiated by UV light except for the sample prepared at $r = 20$. It can be also observed from Fig. 1 that the diffraction peaks of the samples prepared with photo-irradiation are sharper than those of the samples prepared without irradiation in most cases, indicating the higher degree of crystallinity of these photo-irradiated samples. Table 1 gives the crystallite sizes of TiO_2 calculated by

using the Scherrer equation. Photo-irradiation and hydrolysis ratio seem to have not apparent effects on the crystallite size. Moreover, it is interesting to note that the diffraction peaks originated from rutile are much sharper than that from anatase in sample R20-P (Fig. 1), and the calculated crystallite size of the rutile is larger than that of the latter. This suggests the possible growth of rutile from the primary anatase particles.

TEM observation (Fig. 2a) reveals that the sample R10-P consists of the agglomerates of primary particles of 5–7 nm, which is in general agreement with the XRD determinations. The particles are randomly oriented and exhibit irregular shapes. In contrast, more agglomerated and amorphous samples acquired for R10-N made it difficult to observe primary particles in HRTEM. The selected area electron diffraction patterns of R10-N (Fig. 2b) and R10-P (Fig. 2c) also confirm higher crystallinity of R10-P than R10-N. Diffraction rings in the patterns indicate that both samples are polycrystalline.

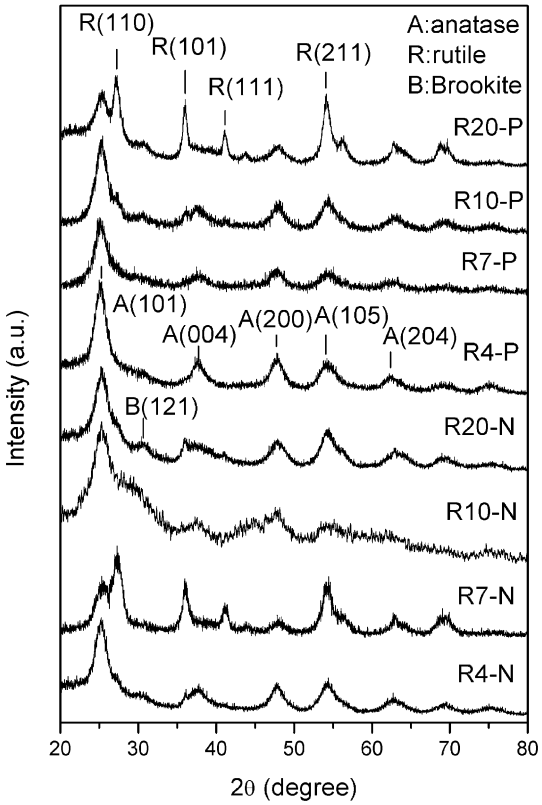

Fig. 1. XRD patterns of TiO_2 powders prepared at various hydrolysis ratios followed by annealing at 373 K.

R7-N and R7-P were selected for further investigation in the following studies since photo-irradiation changed the crystalline phase greatly at hydrolysis ratio of 7. XPS analysis was used to determine the surface properties of TiO_2 nanoparticles prepared by the two different methods. The XPS spectra of Ti 2*p* of both samples (not shown) only show two peaks located at 458.6 and 464.2 eV, indicating that titanium exists as the chemical state of Ti^{4+}. No other chemical states of Ti can be found. The O 1*s* core level spectra are asymmetric as shown in Fig. 3a and c. Besides the main peak located at 529.9 eV attributed to lattice O^{2-}, a shoulder at higher binding energy of 532.3 eV, corresponding to other oxygen species on the surface such as hydroxyl groups, oxygen in the carbon–oxygen bonds (C–O and O═C–O), etc., can be clearly seen for both samples. In the C1*s* spectra (Fig. 3b and d), both samples exhibit a dominant peak at 284.4 eV, attributed to the contribution of C–C and C–H bonds. The component at ca. 286.3 eV corresponds to C–O contribution originates from unhydrolyzed alkyls groups, by-product of hydrolysis reaction and solvent molecules adsorbed on the particle surface. In addition to that, the shoulders at high binding energy side identified for both samples should be assigned to O═C–O, which probably comes from chemisorbed CO_2. The detailed comparison including peak position, full-width of half-maximum (FWHM) and relative contents of the surface species calculated from deconvolution of both samples are shown in Table 2. The atomic ratio of Ti^{4+} to lattice O^{2-} is 1:2 as expected for TiO_2 in both of the samples. From Table 2, we can see that the relative content of surface oxygen species of sample R7-P is lower than that of sample R7-N. Accordingly, the total content of C species in the forms of C–O (8.7%) and O═C–O (2.8%) of R7-P is much lower than that (13.7% and 3.15%) of the sample R7-N. This means that UV irradiation decreases carbonaceous species on the surface of TiO_2 nanoparticles. Generally, these impurities will occupy the active sites on the particle surface and are harmful for the function of TiO_2 in some applications, such as photocatalytic detoxification [27]. Furthermore, the less presence of C–O species in sample R7-P also proves the promotion of UV irradiation on hydrolysis reaction.

The incomplete hydrolysis and condensation of TiO_2 is also confirmed by the thermogravimetry (TG) curve illustrated in Fig. 4. Below 100 °C, a mass loss of about

Table 1
The crystallite sizes of TiO_2 powders prepared at various hydrolysis ratios followed by annealing at 373 K

Sample	R4-N	R7-N	R10-N	R20-N	R4-P	R7-P	R10-P	R20-P
Crystallite size (nm)	8.2	8.5(A)[a] 8.6(R)[b]	8.5	8.2	8.1	8.3	7.2	9.0(A) 11.3(R)

[a]A: anatase.
[b]R: rutile.

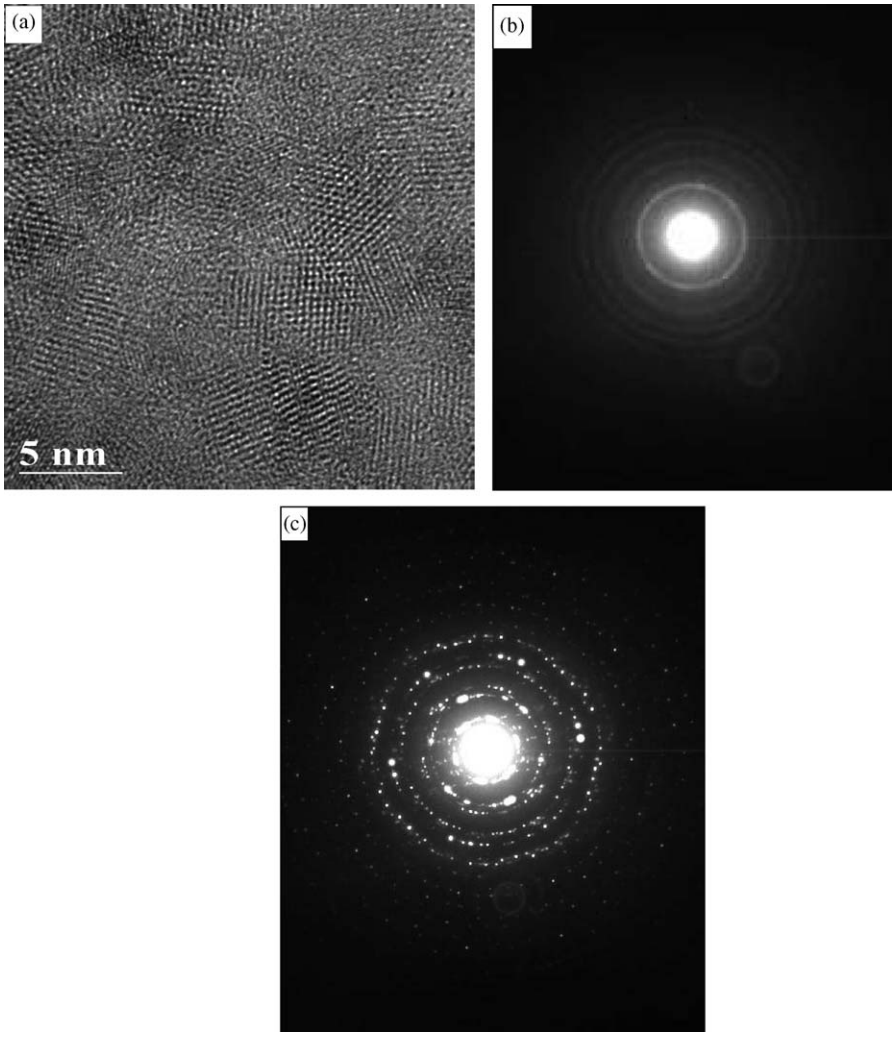

Fig. 2. HRTEM photograph of R10-P (a) and selected area electron diffraction patterns of samples R10-N (b) and R10-P (c) annealed at 373 K.

4.5% for R7-N and 8.4% for R7-P can be observed, corresponding to the removal of physisorbed H_2O and alcohols. From 100 to 400 °C, the weight loss should be attributed to the removal of strongly adsorbed H_2O, surface hydroxyl and the thermal decomposition of residue organic species according to XPS results. The weight loss less than 1% above 400 °C may originate from the decomposition of trace residue species related to O═C–O. Evidently, sample R7-P experienced more weight loss than sample R7-N. Considering the fewer amounts of C–O species in sample R7-P supported by XPS analysis, the difference most probably comes from the different amount of adsorbed H_2O and surface hydroxyl between the two samples. This is further substantiated by the observation of the largest difference in mass loss occurring below 100 °C.

Ultraviolet irradiation was found to accelerate the phase transition from anatase to rutile in our previous study due to the formation of Ti^{3+} under irradiation [28]. So the phase transition processes of R7-P and R7-N were further investigated and the XRD patterns are presented in Fig. 5. Obviously, photo-irradiation does not accelerate the phase transition in this case, in accordance with the absence of Ti^{3+} in XPS spectra. Sample R7-P (Fig. 5b) undergoes the phase transition from anatase to rutile over a wide range of temperature region from 573 to 973 K, indicating the low thermal stability of anatase herein. Similarly, pure rutile can only be acquired at 973 K for sample R7-N although rutile coexists with anatase even at 373 K (Fig. 5a). Table 3 gives the detailed crystallite sizes, phase contents, specific surface areas and pore sizes of R7-N and R7-P calcined at different temperatures. Photo-irradiation has not affected the crystallite sizes significantly throughout all of the temperatures as shown in Table 3. However, specific surface areas (S_{BET}) can be improved by photo-irradiation. The largest S_{BET} value of 172 is observed for the sample prepared by a photo-assited sol–gel process followed by calcination at 473 K. The increase in specific surface areas for both samples when the calcination temperature is increased from 373 to 473 K appears to be partly due to the change in the surface morphology with desorption of

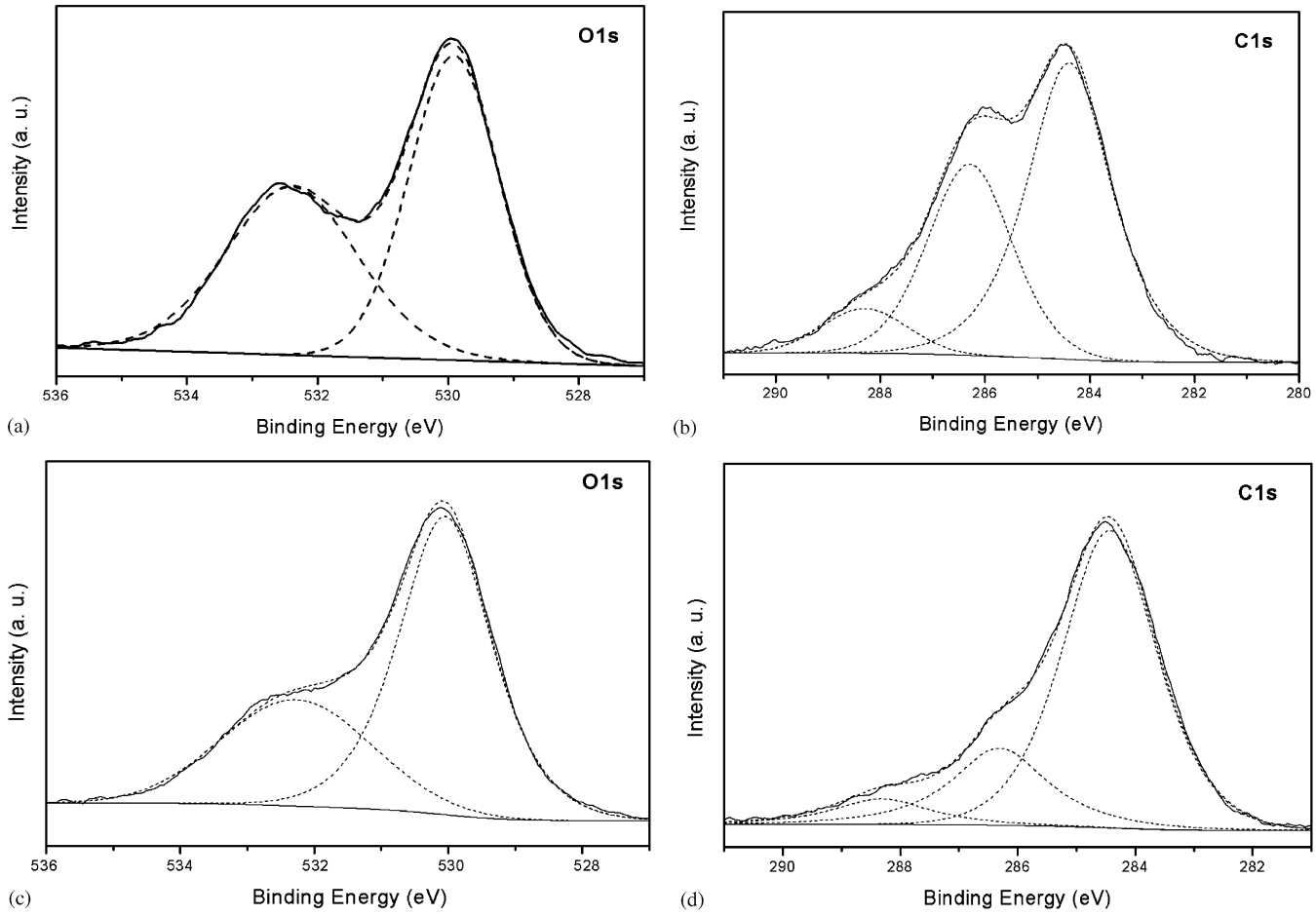

Fig. 3. The O 1*s* and C 1*s* core level spectra of R7-N (a, b) and R7-P (c, d) annealed at 373 K.

Table 2
The peak position (eV), FWHM, and quantification[a] of the surface species on the samples R7-N and R7-P annealed at 373 K

Sample	Ti2*p*		O1*s*		C1s			Cl 2*p*	N1*s*
	Ti2$p_{3/2}$	Ti2$p_{1/2}$	Lattice O^{2-}	Other species	–C–H–	–C–O–	O=C–O		
R7-N									
Peak position (eV)	458.6	464.2	529.9	532.4	284.4	286.3	288.3	197.8	399.7
FWHM	2.0	2.7	1.63	2.39	1.9	1.9	1.9	1.84	1.43
Content (%)	12.5		25.1	20.1	23.0	13.7	3.15	1.99	0.550
R7-P									
Peak position (eV)	458.6	464.2	530.0	532.3	284.4	286.3	288.3	198.7	398.9
FWHM	2.0	2.7	1.63	2.64	1.9	1.9	1.9	1.82	1.74
Content (%)	13.2		26.5	14.4	30.3	8.70	2.80	3.56	0.520

[a]The percentage contents are determined by the integrated peak areas after being calibrated by the response coefficients (O1*s*: 2.93, C1*s*: 1.00 and Ti2*p*: 7.91, Cl2*p*:2.29, N1*s*: 1.80).

chemisorbed H_2O or other small organic molecules. Above 573 K, S_{BET} decreases monotonically with the increase of calcination temperature due to crystallite growth. For both samples, the pores exhibit monomodal distribution at different calcination temperatures. The pore sizes lie in the microporous region for both powders acquired at 373 K and shift to mesoporous region (3.0–7.5 nm) at elevated temperatures, indicating the growth of pores caused by crystallization. At the same time, the distribution of pores (not shown) broadens with the increase of calcination temperature due to the formation of interaggregated pores.

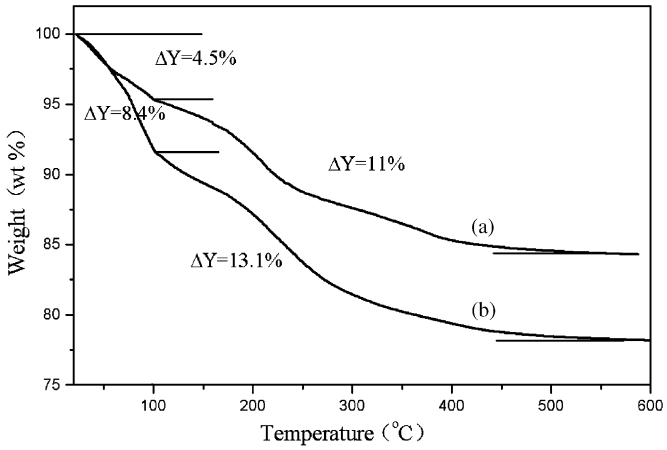

Fig. 4. TGA traces of the samples R7-N (a) and R7-P (b) annealed at 373 K.

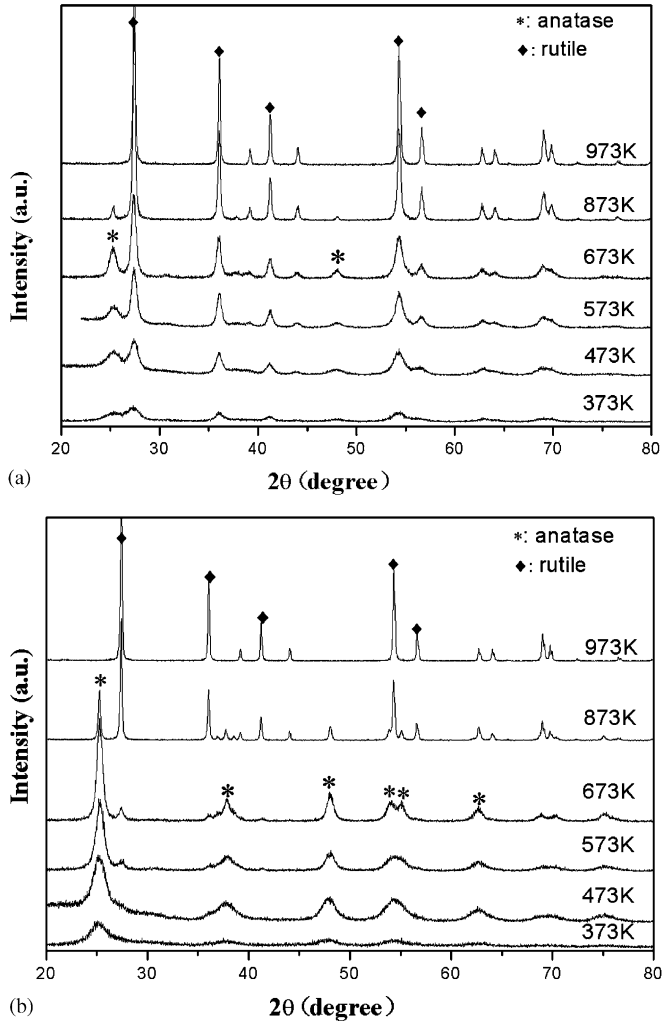

Fig. 5. XRD patterns of the samples R7-N (a) and R7-P (b) annealed at various temperatures.

It is well known that titania naturally occurs in three mineral forms: anatase, rutile, and brookite. $[TiO_6]$ octahedron is the fundamental structure units in the three TiO_2 crystals. In the rutile structure each octahedron is in contact with 10 neighbor octahedrons (two sharing edge oxygen pairs and eight sharing corner oxygen atoms) while in the anatase structure each octahedron is in contact with eight neighbors (four sharing an edge and four sharing a corner) [29]. The structure of brookite is more complicated and will not be discussed here. The following plausible crystallization process may explain this unusual effect of ultraviolet irradiation. It has been widely studied and accepted that the chemistry involved in sol–gel process is based on hydrolysis and condensation reactions [Eqs (1)–(3)] of metallo-organic compounds [30,31] such as titanium alkoxides $(Ti(OR)_4)$:

$$Ti-OR + H_2O \rightarrow Ti-OH + R-OH \quad \text{Hydrolysis,} \qquad (1)$$

$$Ti-OH + Ti-OX \rightarrow Ti-O-Ti + X-OH \quad (X = H \text{ or } X = R) \quad \text{Oxolation,} \qquad (2)$$

$$Ti-OH + Ti-OH \rightarrow Ti-(OH)_2-Ti \quad \text{Olation.} \qquad (3)$$

In terms of the partial charge model proposed by Henry and Livage [32], the coordination number of titanium changes from 4 to 6 early in the hydrolysis process, and that the basic building unit in the polymerization process is an octahedral arrangement of the oxygen atoms around a titanium centre. In the reaction performed in an acidic medium, 6-fold structure units of $[Ti(OH)_x(OH_2)_{6-x}]^{(4-x)+}$ undergo condensation and become the octahedra that are incorporated into the final crystal structure [33]. If an olation pathway dominates the condensation process, condensation can proceed along apical directions, leading to the skewed chains of the anatase structure. While oxolation leads to linear growth along the equatorial plane of the cations, and this reaction, followed by oxolation between the resulting linear chains, leads to rutile formation. Such condensation processes have been discussed in details by Henry and Livage [30,32]. At low hydrolysis ratio ($r = 4$), more isopropoxy groups retain since the hydrolysis is usually incomplete and the fourth alkoxy group is difficult to remove [34–36]. Oxolation leading to rutile linear chain may be unfavorable due to the steric hindrance and accordingly olation occurs to form the skewed chains of the anatase structure in this case. When hydrolysis ratio increases, hydrolysis reaction is nearly completed, condensation proceed simultaneously by oxolation or olation pathway, the competition of the two pathways leads to the coexistence of anatase and rutile in the final product. With the further increase of hydrolysis ratio ($r \geqslant 10$), promotion of hydrolysis leads to the generation of a great amount of hydroxyl groups, which are favorable for olation and result in the anatase structure. It is widely suggested that ultraviolet irradiation can excite and weaken the Ti–OR bonds, thus promoting the hydrolysis reaction, i.e., the replacement of the alkyl groups by hydroxyl groups [18,21,22–24]. As a result, olation is expected to occur when ultraviolet irradiation is introduced in the sol–gel process at various hydrolysis

Table 3
The crystallite sizes, phase contents (%), specific surface areas, and pore sizes of samples R7-N and R7-P annealed at different temperatures

Sample	T/K	Crystallite size (nm)		Phase content (%)[a]		Pore size (nm)	S_{BET} (m^2/g)
		Anatase	Rutile	Anatase	Rutile		
R7-N	373	8.5	8.3	12.9	87.1	2.09	132
	473	8.8	10.0	26.2	73.8	3.59	158
	573	9.5	13.1	18.9	81.1	6.30	91.6
	673	12.8	15.8	24.1	75.9	7.76	74.2
R7-P	373	8.3	—	100	—	2.06	157
	473	8.7	—	100	—	3.50	172
	573	10.4	12.5	90.7	9.3	6.04	100
	673	13.0	18.1	92.8	7.2	7.45	80.3

[a]The phase content was calculated according to the method reported in Ref. [26].

ratios. Faster reaction rate has already been confirmed to be favorable for anatase in the hydrolysis of titanium alkoxide in an acid solution [33]. However, at high hydrolysis ratio ($r = 20$), rutile seems more like to grow from anatase particles formed at early reaction process according to XRD analysis. On the one hand, it has been suggested that the enhanced surface hydroxylation combined with the highly distorted bulk atomic arrangement of the anatase make it thermodynamically less stable [37]. On the other hand, it is well known that the concentration of OH groups on the surface of TiO_2 increases by UV illumination [38,39]. According to TGA analysis, surface hydroxylation of the samples prepared by a photo-assisted sol–gel method has been improved by photo-irradiation. At such a high hydrolysis ratio, the initial reaction product is more probably to be anatase with a significant amount of hydroxyl groups due to the accelerated hydrolysis and condensation. The surface of titania becomes protonated in the acid medium, which allows a dissolution precipitation mechanism to operate, resulting in the formation of rutile [37,40].

In our previous work, when the conventional sol–gel derived precipitates are amorphous in nature, nanoparticulate anatase TiO_2 can be obtained using a photo-assisted sol–gel method under the otherwise same conditions [22–24]. We found that the oxygen vacancies induced by UV illumination on colloid accelerate the phase transformation of amorphous to anatase phase in that case [23,24]. On the basis of the arguments above, it seems reasonable to suggest that photo-irradiation favors the formation of anatase, as a result of more hydroxyl groups generated or oxygen vacancies formed under illumination. The increase in hydroxyl groups will further accelerate the phase transformation of anatase to rutile at high hydrolysis and condensation rates. By changing the reaction rate, the crystalline phase and surface properties of TiO_2 may be finely controlled by using this photo-assisted sol–gel method.

We also evaluated the photocatalytic activity of the TiO_2 samples prepared by the two different methods by photodegradation of the organic dye molecule RB, a dye often used as a tunable laser dye because of its stable photochemical properties. The degradation results are depicted in Fig. 6. It is clearly shown that the photolysis of RB under the used condition is very slight (blank) and thus the excitation of the dye can be neglected compared with the excitation of TiO_2. For the sample prepared with UV irradiation, the dye molecules are almost degraded completely within 60 min while only about 80% of the dye is degraded by the sample prepared without UV irradiation, indicating that the activity of the sample prepared with photo-irradiation is higher. The higher photocatalytic activity of the sample R7-P is probably attributed to the larger surface area, higher degree of crystallinity, and the less deleterious species on the surface.

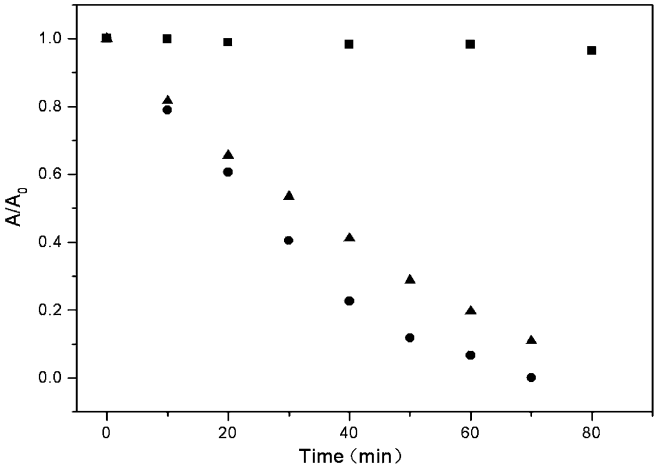

Fig. 6. The photolysis (■) and photocatalytic degradation of RB in TiO_2 suspensions of R7-N (▲) and R7-P (●) calcined at 373 K. A: the absorbance of RB at 554 nm after irradiation for various times. A_0: the absorbance of RB at 554 nm before irradiation.

4. Conclusion

Nanosized titania was prepared by photo-assisted and conventional sol–gel methods at various hydrolysis ratios.

The crystallization behavior and surface microstructures were greatly affected by photo-irradiation. The exclusive anatase crystal acquired by the photo-assisted sol–gel method in most cases can be explained by considering a condensation process dominated by an olation pathway, which is seemingly favored under UV irradiation. More surface hydroxyl groups remained in the photo-irradiated sample at high hydrolysis ratio led to the phase transformation of the sample from anatase to rutile structure in part. Larger surface area and less carbonaceous species can be acquired by this photo-assisted sol–gel method, which resulted in the relative high photocatalytic activity of TiO_2. By this method, fine control of sol–gel processing parameters under irradiation may be helpful to prepare anatase and rutile titania with high crystallinity and improved properties.

Acknowledgments

This work was supported by National Natural Science Foundation of China (Nos. 50221201, 90301010, 20373077, 20471062), the Chinese Academy of Sciences and the National Research Fund for Fundamental Key Projects No. 973.

References

[1] J.L. Gole, J.D. Stout, J. Phys. Chem. B 108 (2004) 1230.
[2] M.I. Baraton, L. Merhari, J. Eur. Ceram. Soc. 24 (2004) 1399.
[3] G. P. Fotou, S. Vemury, S.E., Pratsinis, Chem. Eng. Sci. 49 (1994) 4939.
[4] Y. Ma, J.B. Qiu, Y.A. Cao, Z.S. Guan, J.N. Yao, Chemosphere 44 (2001) 1087.
[5] S.F. Yang, Y.H. Liu, Y.P. Guo, J.Z. Zhao, H.F. Xu, Z.C. Wang, Mater. Chem. Phys. 77 (2002) 501.
[6] W. Zhang, Y. Li, S. Zhu, F. Wang, Catal. Today 93–95 (2004) 589.
[7] G. Sivalingam, M.H. Priya, G. Madras, Appl. Catal. B 51 (2004) 67.
[8] J.E. Lee, S.M. Oh, D.W. Park, Thin Solid Films 457 (2004) 230.
[9] S.J. Lee, C.H. Lee, Mater. Lett. 56 (2002) 705.
[10] S.H. Lee, M. Kang, S.M. Cho, G.Y. Han, B.W. Kim, K.J. Yoon, C.H. Chung, J. Photochem. Photobiol. A 146 (2001) 121.
[11] C.-C. Wang, J.Y. Ying, Chem. Mater. 11 (1999) 3113.
[12] J. Ovenstone, K. Yanagisawa, Chem. Mater. 11 (1999) 2770.
[13] J.C. Yu, J.G. Yu, W.K. Ho, L.Z. Zhang, Chem. Comm. 19 (2001) 1942.
[14] Y. Zhou, C.Y. Wang, Y.R. Zhu, Z.Y. Chennnnn, Chem. Mater. 11 (1999) 2310.
[15] K. Naoi, Y. Ohko, T. Tatsuma, J. Am. Chem. Soc. 126 (2004) 3664.
[16] A.V. Dijken, A.H. Janssen, M.H.P. Smitsmans, A. Meijerimk, Chem. Mater. 10 (1998) 3513.
[17] A.V. Dijken, D. Vanmaekelbergh, A. Meijerink, Chem. Phys. Lett. 269 (1997) 494.
[18] H. Imai, M. Yasumori, H. Hirashima, J. Appl. Phys. 11 (1996) 79.
[19] H. Imai, H. Morimoto, K. Awazu, Thin Solid Films 351 (1999) 91.
[20] J.-Y. Zhang, L.-J. Bie, V. Dusastre, I.W. Boyd, Thin Solid Films 318 (1998) 252.
[21] T. Nagase, T. Ooie, J. Sakakibara, Thin Solid Films 357 (1999) 151.
[22] Z.S. Guan, X.T. Zhang, Y. Ma, Y.A. Cao, J.N. Yao, J. Mater. Res. 16 (2001) 1.
[23] H.M. Liu, W.S. Yang, Y. Ma, Y.A. Cao, J.N. Yao, New J. Chem. 26 (2002) 975.
[24] H.M. Liu, W.S. Yang, Y. Ma, Y.A. Cao, J.N. Yao, J. Zhang, T.D. Hu, Langmuir 19 (2003) 3001.
[25] H. Cheng, J. Ma, Z. Zhao, Chem. Mater. 7 (1995) 663.
[26] H.Z. Zhang, J.F. Banfield, J. Phys. Chem. B 104 (2000) 3481.
[27] S.S. Watson, D. Beydoun, J.A. Scott, R. Amal, Chem. Eng. J. 95 (2003) 213.
[28] H.M. Liu, W.S. Yang, Y. Ma, X.F. Ye, J.N. Yao, New J. Chem. 27 (2003) 529.
[29] A.L. Linsebigler, G.Q. Lu, J.T. Yates Jr., Chem. Rev. 95 (1995) 735.
[30] J. Livage, M. Henry, C. Sanchez, Prog. Solid State Chem. 18 (1988) 259.
[31] A. Chemseddine, T. Moritz, Eur. J. Inorg. Chem. (1999) 235.
[32] M. Henry, J.P. Jolivet, J. Livage, Struct. Bond. (Berlin) 77 (1992) 155.
[33] M. Gopal, W.J. Moberly Chan, L.C. De Jonghe, J. Mater. Sci. 32 (1997) 6001.
[34] J. Blanchard, M. In, B. Schaudel, C. Sanchez, Eur. J. Inorg. Chem. (1998) 1115.
[35] M.J. Velasco, F. Rubio, J. Rubio, J.L. Oteo, Thermochim. Acta 326 (1999) 91.
[36] R.R. Bacsa, M. Gratzel, J. Am. Ceram. Soc. 79 (1996) 2185.
[37] H.S. Jung, H. Shin, J.-R. Kim, J.Y. Kim, K.S. Hong, J.-K. Lee, Langmuir 20 (2004) 11732.
[38] A. Nakajima, S. Koizumi, T. Watanabe, K. Hashimoto, Langmuir 16 (2000) 7048.
[39] N. Sakai, A. Fujishima, T. Watanabe, K. Hashimoto, J. Phys. Chem. B 105 (2001) 3023.
[40] K. Yanagisawa, J. Ovenstone, J. Phys. Chem. B 103 (1999) 7781.